COMPUTATIONAL SIMULATION OF SPHERICAL DIFFUSION FLAME DYNAMICS AND EXTINCTION IN MICROGRAVITY

By

TIANYING XIA

A thesis submitted to the

Graduate School-New Brunswick

Rutgers, The State University of New Jersey

In partial fulfillment of the requirements

For the degree of

Master of Science

Graduate Program in Mechanical and Aerospace Engineering

Written under the direction of

Professor Stephen D. Tse

And approved by

_____

_____

_____

New Brunswick, New Jersey

JANUARY 2015

ABSTRACT OF THE THESIS

COMPUTATIONAL SIMULATION OF SPHERICAL DIFFUSION FLAME DYNAMICS AND EXTINCTION IN MICROGRAVITY

By TIANYING XIA

Thesis Director:

Stephen D. Tse

Spherical diffusion flame experiments in microgravity are slated to be conducted on the space station in the near future. The basic flame configuration adopted for the investigations is the spherically-symmetric diffusion flame generated by issuing a fuel mixture into a quiescent oxidizing environment. Upon ignition, the flame is initially located close to the burner surface, subsequently moving outward to reach the steady-state location. $H_2/CH_4/N_2$ and H_2/CH_4/He mixtures are examined in the test matrix. Therefore, to guide the experiments, computational simulations are performed with detailed chemistry and transport, along with optically thick and optically thin radiation models, as well as with no radiative loss.

Such flames allow for the investigation of transient flame extinction at the two limits: i.e. radiative and kinetic. A high flow rate can result in a maximum extinction Damkhőler number (*Da*) beyond which burning is not possible, caused by the reduction in the flame temperature due to radiative heat loss. By transitioning from a moderate flow rate (for which a diffusion flame can be established) to a low flow rate, a minimum extinction *Da* may be reached, corresponding to the purely kinetic limit of burning. The dual diffusion flame extinction modes for specific mixture compositions and initial ambient oxygen concentrations are obtained numerically.

ACKNOWLEDGEMENTS

I am very sincerely grateful to my advisor, Prof. Stephen D. Tse for all the advices and guidance. His insightful directions and purposes helped me overcome many difficulties throughout the project. Without his support, I would not had achieved this far. I would also like to thank Prof. Bagchi and Prof. Shan for their valuable time on reviewing and improving my work during the winter holiday.

Furthermore, I would like to thank to my secondary advisor Dr. Gang Xiong who has contributed tremendously to my work. He helped me modify the code and diagnose problems throughout the project. He is always willing to hold discussions with me and guide me with patience. Special thanks to Hua for providing his opinions on the project and offering great ideas. I am also grateful to Dr. Tianfeng Lu at University of Connecticut for providing me with some simulation codes. I also want to thank Yuqian for his encouragement. Lastly, I would like to than Dr. Zhizhong Dong for his help during my research.

The support from NASA Grant NNX11AP44A is gratefully acknowledged.

Last, but not least, I would like to thank my parents for everything. There is nothing more important to me than to have your love and support.

TABLE OF CONTENTS

LIST OF TABLES

LIST OF ILLUSTRATIONS

Chapter 1

Introduction

Human beings have never stopped exploring space since thousands of years ago. In recent decades, people all over the world are spending more time and money on space-based research. Microgravity combustion is a crucial subject with respect to spacecraft safety. Fundament combustion studies under microgravity conditions offer us a better understanding of combustion science by introducing gravity-free investigation of physical and chemical processes.

In this work, one-dimensional spherical diffusion flame behaviors in microgravity, particularly kinetic and radiative extinctions, have been studied.

1.1. Scientific background

Convection between warm and cool air are due to the temperature gradient. Similarly, under the earth's gravitational condition, gaseous density differences generate buoyancy forces which drive the flow. Both gas velocity and temperature decrease radially outward from the hot products of combustion through cold mixtures. These phenomena can be explained in the governing equations for mass, momentum, energy and species. Buoyant forces on earth greatly complicate the convective-diffusive transport

processes which affect the transport of thermal energy, reactants and products. Multi-dimensional flame configurations under gravitational field bring difficulties to both experimental and computational research. [1] Many computational and analytical calculations consider buoyant forces negligible, which can be far from correct.

Figure 1.1: Spherical diffusion flame images from 5.0-s drop tower, showing the onset of radiative extinction.[2]

Spherical diffusion flames can be established in buoyancy-free conditions. Note that the cylindrical diffusion flame does not possess a steady-state solution. The absence of buoyancy-induced flows in microgravity environment greatly increases the reactant residence time. Parametric studies involving residence time provides an ideal manner to access flame chemistry, which helps to understand complex combustion process like ignition and extinction.[3] As shown in Figure 1.1, diffusion flame is close to sphere in the microgravity condition. Spherically-symmetric flames can be considered as one-dimensional, which significantly simplifies their study, especially for their profiles and sizes. The one-dimensional and steady state flame should correspond to the simplest flow configuration. However, there is no mathematical steady solution for diffusion flames for the planner and

cylindrical geometries in the semi-infinite domain. The only possible one-dimensional and steady flame is the spherical flame.

Chemical kinetics is the study of rates of a chemical reaction, which is useful for determining how a reaction occurs. Flames will propagate and sustain when the reactions are quickly enough through certain chemical mixtures.

1.2. Microgravity combustion research review

One of the first books published on microgravity combustion is entitled Combustion Experiments in a Zero-Gravity Laboratory, edited by Thomas H. Cochran [4]. The authors presented many great ideas on investigating combustion in microgravity. However, the book offered very little experimental data and detailed models. Ever since then, people began to conduct research on microgravity combustion which has revealed many distinct fundamental aspects of combustion phenomena. Microgravity combustion has been studied both experimentally and numerically. Microgravity conditions are commonly created in ground-based facilities, such as in drop tower and, parabolic flight aircraft. Space based research has been conducted on the space shuttle and International Space Station.

In premixed-gas flames, fuel, oxidant and inert gases have been mixed before combustion is initiated. Since 1985, Prof. Ronney has conducted experiments on premixed flames at low gravity conditions.[5] Law and Faeth[6]

addressed the opportunities to improve understandings on microgravity combustion phenomena including stretched flames, flamefront instabilities, flammability limits and near-limit phenomena of gaseous premixed flames. Other combustion propagation phenomena include smoldering and materials, where heterogeneous reactions or completely solid-state reactions occur.

Atreya and his collaborators [7, 8] presented the theoretical and experimental results for radiative extinction of one-dimensional unsteady diffusion flames in microgravity conditions. He and his collaborators set up the experiments in the NASA Glenn Research Center 2.2s drop tower. In the experiments, flame radius, flame temperature and soot formation was measured.

Sunderland and Axelbaum[9] also investigated spherical diffusion flames in microgravity conditions using the NASA Glenn Research Center 2.2s drop tower. Experimental and numerical results together showed that their flames did not reach steady state during 2.2 seconds. They found that the differences between adiabatic flame temperature and actual peak temperature are mainly due to gas-phase radiative heat loss. Sooting process were also studied.

Mills and Matalo [10] have examined the structure and extinction characteristics of burner-generated spherical diffusion flames analytically. They discovered a maximum flow rate above which the steady flame cannot be sustained due to radiative loss and a minimum flow rate below which the steady flame cannot be sustained due to short resistance time. The results also

indicated that the flame temperature at low mass flow rate limit is typically 400-700 K higher than the flame temperature at high mass flow rate limit, which is radiative extinction limit.

Tse et al. conducted experiments on burner-generated spherical diffusion flames by issuing H_2/CH_4/inert gas mixtures into atmospheric air in the same 2.2s drop tower.[1] They used a computational model with a statistical narrow band radiation model. Both experimental and computational results showed that for the fuel mixtures and mass flow rates tested, spherical diffusion flames did not reach steady state in 2.2 seconds microgravity. The computational model with detailed chemical and transport predicted the radiative extinction time to be more than 2.2 seconds.

Christiansen et al.[11] numerically investigated thermal-diffusively-induced oscillation near the steady-state radiative and kinetic extinction limits, using detailed chemistry and transport for methane ($50\%CH_4/50\%$He into $21\%O_2/79\%$He) and hydrogen ($100\%H_2$ into $21\%O_2/79\%$He) diffusion flames. They found that the methane diffusion flame exhibits large amplitude oscillations and low frequency, while hydrogen diffusion flames show relatively small amplitude oscillations and high frequency.

1.3. Diffusion flame extinction

Diffusion flame extinction is usually caused by reactant leakage through the flame front. Damkőhler number (*Da*) is defined as the ratio of the

characteristic residence time to the characteristic chemical reaction time through the flame. As the local *Da* gets low, the spherical diffusion flame tends to extinction via two different mechanisms. At the low flow rate, the flame size is small and the reaction zone is situated in a region of high flow velocity. High flow velocity gives a short residence time in the reaction zone. When *Da* reaches a number low enough that burning is not possible, it called kinetic extinction. At the high flow rate, the spherical diffusion flame size will be larger. Big flame size corresponds to more radiative heat loss. Increasingly heat loss due to radiation lowers the flame temperature, increasing the chemical reaction time and resulting in radiative extinction.

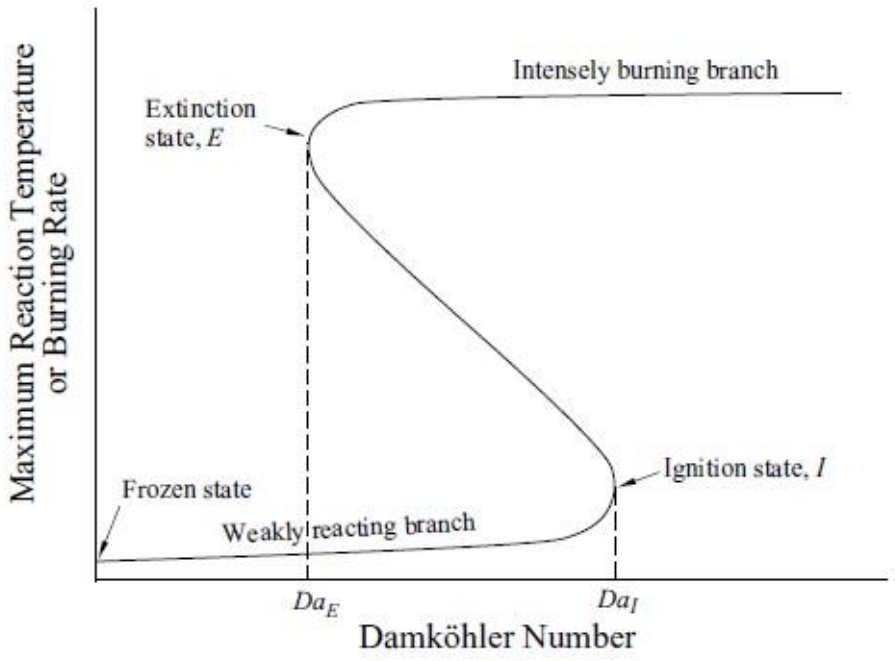

Figure 1.2: S-curve with distinct ignition and extinction states.[12]

Figure1.1 is the maximum temperature versus the system Damkőhler Number, *Da*. When *Da* increases from the frozen state until the first critical point, Da_I, there are non-self-sustained weak reactions, leading up to ignition. At ignition, the processes jump to the upper branch corresponding to fast reactions and intense self-sustained burning. When decreasing the Damkőhler Number along the upper branch, a minimum value *Da* is reached (at the turning point of the curve), which corresponds to the extinction Damkőhler Number. The turning points physically means that there are the moments existing when the chemical reaction rate and the heat transport rate cannot be balanced in steady state.[9] Note that the ignition and extinction turning points correspond to different *Da*, manifesting the hysteresis in the associated flame behavior. The middle portion of the curve in between the turning points represents mathematically steady solutions, but they are unstable, and are thus not physically realizable.

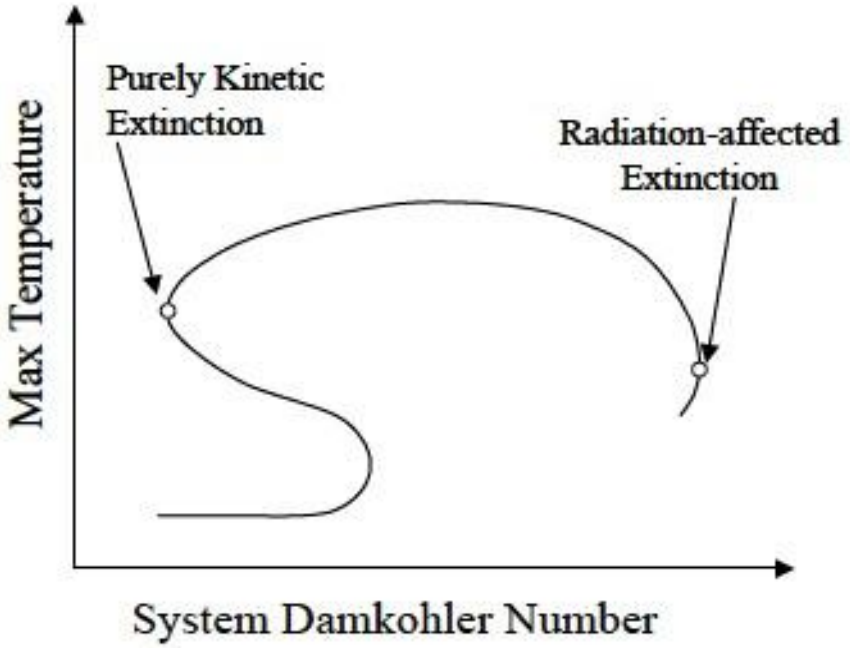

Figure 1.3: Modified S curve for Radiative Extinction, as a function of System *Da* number.[2]

Tien[13] and Chao et al.[14] applied theoretical analysis of diffusion flame extinction with flame radiation. Their results showed the existence of another flame extinction point, which is caused by radiative heat loss as shown in Figure 1.2. There is a maximum extinction *Da* (system) above which burning is also not possible. When the flame size increases, the heat loss due to radiation will also increase. As a result, the flame temperature drops until the flame extinguishes, which we have discussed earlier.

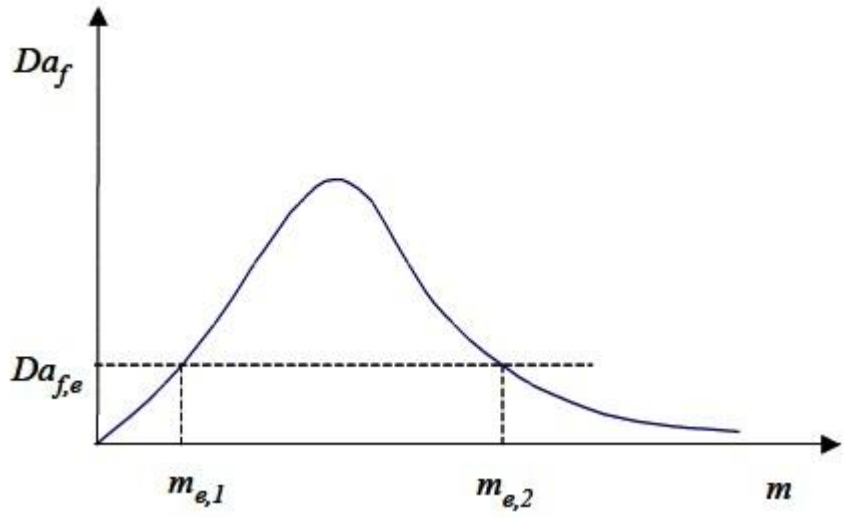

Figure 1.3: Local Damkőhler Number versus mass flow rate.[10]

Based on the analyses of Law and Tse[12], the local Damkőhler Number (in the flame region) for the burner-generated spherical diffusion flame can be derived to be proportional to $m^2\exp(-Am^2)$, where m is the mass flow rate, and A is a constant[10]. Note that for the present spherical diffusion flame, $m \sim d_f$, where d_f is the flame diameter. The m^2 in the coefficient term is proportional to the characteristic diffusion time, and the exponential term is inversely proportional to the characteristic chemical reaction time. As shown in Figure 1.3, a single extinction *Da* (local), corresponds to two mass flow rates, $m_{e,1}$ and $m_{e,2}$. When m is at lower value $m_{e,1}$, m^2 is the dominant term, which represents purely kinetic extinction. When m is at the higher value $m_{e,2}$, $\exp(-Am^2)$ is the dominant term, which represents radiative extinction. Thus, the local *Da* number is consistent with the canonical extinction criterion of Linan[15]. On the other hand, the system *Da* is defined based on the adiabatic

flame temperature (without radiative loss), which means *Da* is proportional to m^2. As a result, there are two different system *Da* number, i.e. $Da_{e,1}$ and $Da_{e,2}$, which correspond to $m_{e,1}$ and $m_{e,2}$, as shown in Fig. 1.2 and given in the computational results[10].

1.4. Objectives

The ultimate goal of the study is to improve the understanding of diffusion flame processes including dual extinction states and flame dynamics. Spherical diffusion flame study in microgravity plays an important role in space-based fire safety. This computational work will be used to refine the test matrix for the experiments to be performed on the International Space Station. In this work, different fuel/oxidizer/inert gas mixtures and concentrations are used to study the extinction states and extinction times of spherical diffusion flames. Different radiative models are compared for extinction time, flame size, flame temperature, etc. Different mass flow rates are examined to study the extinction states.

Chapter 2

Model Description

This work is a follow-up study of the microgravity spherical diffusion flame experiments conducted by Tse et al.[1] as supported by NASA. It is helpful to briefly introduce experimental setup before the computational model description.

2.1. Introduction to experiments

Previous experiments were performed at the NASA Glenn Research Center 2.2s drop tower, which provides a short duration microgravity condition for the research. A 1.27 cm diameter porous spherical burner was used to issue a fuel mixture into ambient air. Different concentrations and mass flow rate of $H_2/CH_4/N_2$ gas mixtures were investigated. Flame was ignited in normal gravity before the drop. Thermocouples were used to measure both the burner surface and the ambient air temperature.

2.2. Introduction to computational models

The computational study is based on the modification of the Sandia premixed flame code[16] with detailed chemical and transport. In this section, the

numerical method will be discussed for the one-dimensional spherical diffusion flames.

2.2.1. Governing Equation

The thermodynamic pressure is considered to be constant throughout the flow field, and the governing equations are as given below:

$$A\frac{\partial \rho}{\partial t}+\frac{\partial m}{\partial r}=0 \tag{2a}$$

$$\rho A\frac{\partial T}{\partial t}+\dot{m}\frac{\partial T}{\partial r}-\frac{1}{C_P}\frac{\partial}{\partial r}\left(A\lambda\frac{\partial T}{\partial r}\right)+\frac{A}{C_p}\sum_{k=1}^{K}\rho Y_k V_k Cp_k\frac{\partial T}{\partial r}+\frac{A}{C_p}\sum_{k=1}^{K}\dot{\omega}_k h_k W_k+\frac{A}{C_P}\dot{q}_{rad}=0 \tag{2b}$$

$$\rho A\frac{\partial Y_k}{\partial t}+m\frac{\partial Y_k}{\partial r}+\frac{\partial}{\partial r}\left(\rho A Y_k V_k\right)-A\dot{\omega}_k W_k=0 \tag{2c}$$

Equation (2a) is the conservation equation of mass, where A is the surface area, $A=4\pi r^2$, r is radius, ρ the density, m the mass flow rate. Equation (2b) is the conservation equation of energy, where c_P is the heat capacity with constant pressure condition, λ the thermal conductivity of gas mixture, Y_k the mass fraction of the k^{th} species, W_k the molecular weight of the k^{th} species, $\dot{\omega}_k$ the molar chemical production rate per unit volume of the k^{th}

species, h_k the specific enthalpy of k^{th} species, and V_k the diffusion velocity of the k^{th} species given by:

$$V_k = v_k + w_k + V_c \tag{2d}$$

where v_k is the ordinary diffusion velocity, and Curtiss-Hirschfelder[17] gives the approximation:

$$v_k = -D_{km} \frac{1}{x_k} \frac{\mathrm{d}x_k}{\mathrm{d}x} \tag{2e}$$

where X_k is the mole fraction, D_{km} the mixture-averaged diffusion coefficient given by the binary diffusion coefficients D_{kj}:

$$D_{km} = \frac{1 - Y_k}{\sum_{j \neq k}^{k} x_j / D_{kj}} \tag{2f}$$

In equation (2d), w_k is the thermal diffusion velocity for light species only, such as H, H_2, and He, given by:

$$w_k = \frac{D_{km} \Theta_k}{X_k} \frac{1}{T} \frac{\mathrm{d}T}{\mathrm{d}x} \tag{2g}$$

where Θ_k is the thermal diffusion ratio.[18]

In equation (2d), V_c is the correction velocity, function of radius r.[19] $\dot{q}_{rad}$ is the radiative heat loss per unit volume. Equation (2c) is the conservation equation of chemical species.

2.2.2. Numerical Method

Steady-state boundary value problem can be approached by using finite difference approximations. An initial approximation usually has only a few

mesh points. New mesh points are added where the solution changes rapidly after obtaining a solution on the previous mesh points until no additional mesh points are needed to resolve the solution. The key of the solution strategy is that at the beginning, the damped modified Newton algorithm is used to solve the equations. If the Newton algorithm does not converge, time integration is introduced to provide a new point for Newton algorithm, which is closer to the solution, until the solution is in the domain of the convergence. [20]

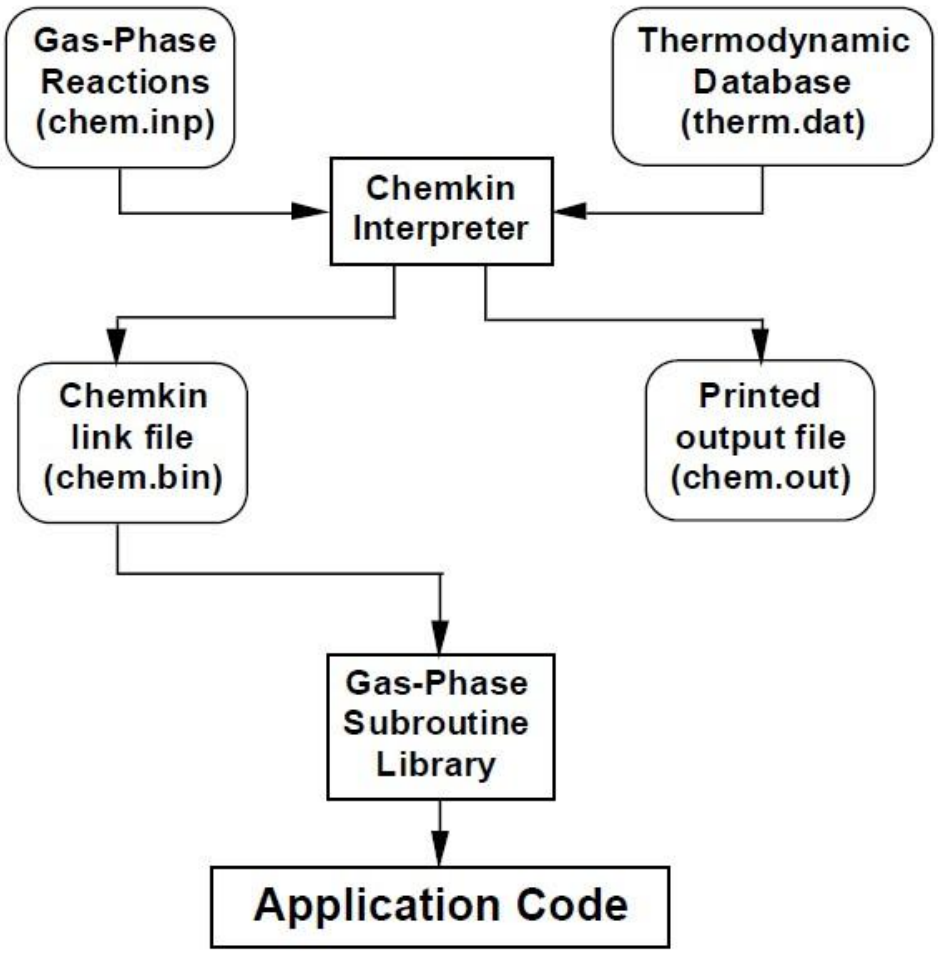

Figure 2.1: Relationship of the diffusion flame code to the CHEMKIN.[21]

Figure 2.1 shows the relationship between the steady one-dimensional spherical diffusion flame code and the CHEMKIN[18] programs. Two input files, chem.inp and therm.dat are the detailed chemical reaction mechanism file and thermodynamic database file, respectively. These two files are processed through Chemkin Interpreter to generate a data file which forms a link to the Gas-Phase Subroutine Library applied in the diffusion flame code. The library has over 100 Fortran subroutines including information on equations of state, thermodynamic properties, and chemical reaction rates.

Similarly, there is another package to generate transport data called TRANSPORT[22] as shown in Figure 2.2. Gas-Phase Subroutine Library and Transport Subroutine Library are linked to the diffusion flame code to provide information that is needed of chemical reaction, thermodynamics, and transport properties for the system.

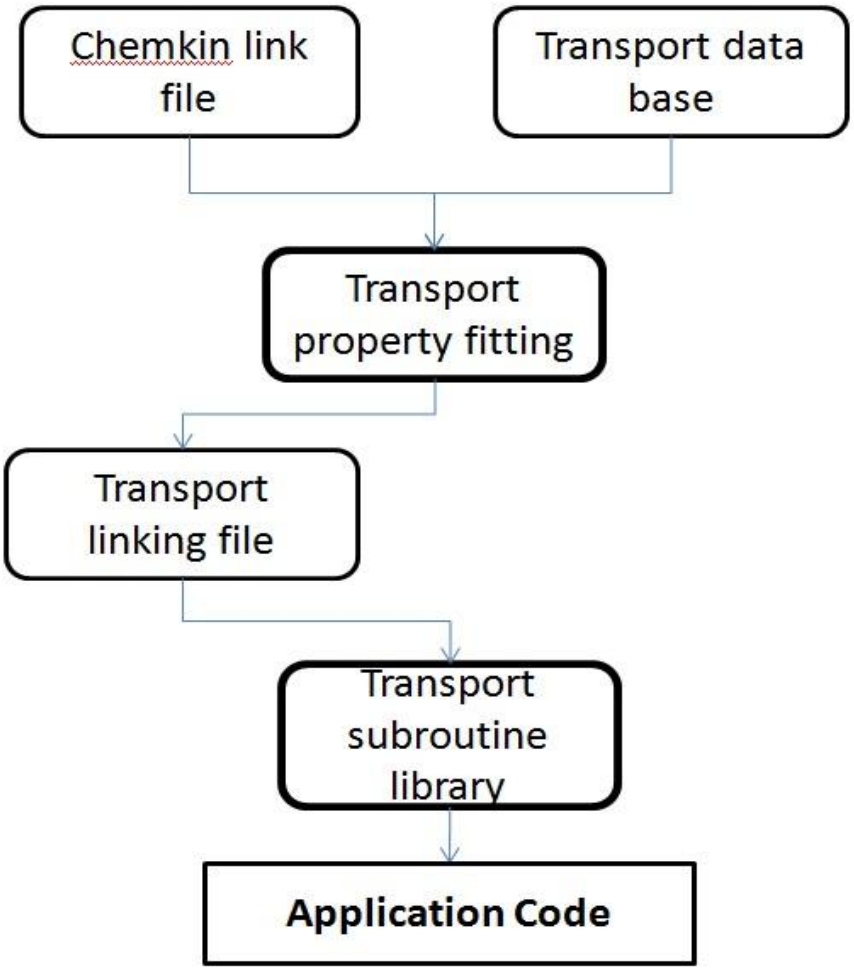

Figure 2.2: Relationship of the diffusion flame code to the TRANSPORT.

The transient diffusion flame code, the main program, is the modification of Sandia Premix code[2]. A modular solver routine TWOPNT[23] is used to solve the boundary value problem. TWOPNT is a program that seeks steady state solutions for systems of one dimensional differential equations. As discussed earlier, TWOPNT is trying to seek for steady state solutions first. If the solution is not in the domain of convergence, the program will add a time step to seek for the transient solutions.

2.2.3. Boundary Condition

In the simulation, the burner size is considered to be 0 cm, by doing this, heat absorption from the burner can be neglected. And the following conditions are applied:

$$p = p_0 , \tag{2h}$$

Equation (2h) is the momentum equation (constant pressure), where p_0 is ambient pressure.

$$T = T_0 \tag{2i}$$

for the issuing mixture.

At the burner surface, mass flux fraction is given as:

$$Y_k = \in_k / \left(1 + \rho V_k A / m_F\right) \tag{2j}$$

where $\in_k$ is the mass fraction of k^{th} species, m_F is the fixed mass flow rate.

At the ambient side, the boundary condition is initially given as 21%O_2/79%N_2.

2.2.4. Initial Condition

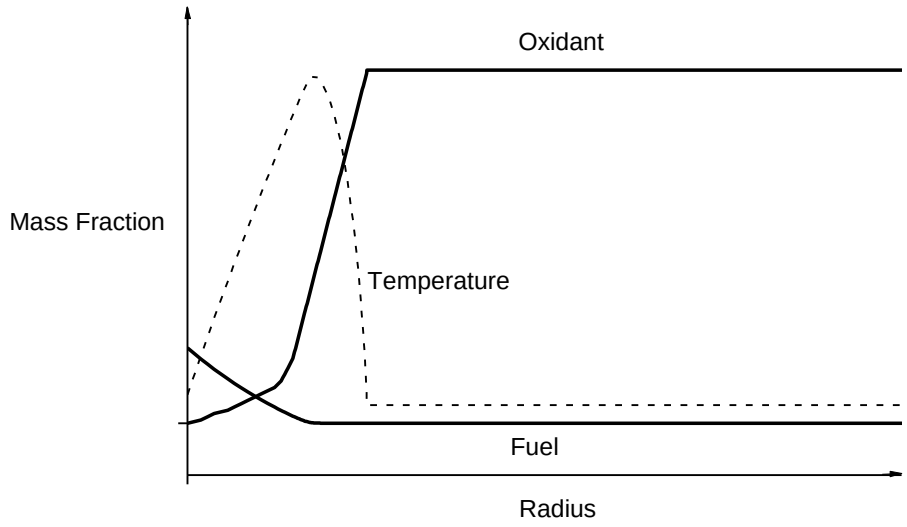

Figure 2.3: The general form of starting estimate.

As the program needs an estimated solution to start, Figure 2.3 shows the general form of starting estimate. For the fuel, usually it is methane, starting from the mass fraction of the gas mixture, and ending up with zero in the infinite long domain of ambient air. For the oxidant, which is usually the oxygen, there is no oxygen in the gas mixture, starting from zero concentration to the mass fraction in air. The exact shape of the initial species profile is not so important as is the confinement of the profile, since the flame is initially ignited locally.

2.2.5. Spatial Discretization

Initial spherical diffusion flames are near the burner surface. As time passes, the flame spreads in the radial direction until eventually the flame extinguishes. A large domain size is needed to obtain a transient behavior for a long period of time. Of course, the domain cannot be infinite in the numerical calculation. As mentioned before, the domain is selected to be 28cm in radius, which corresponds to the size of the chamber to be used in the space-based experiments.

The program provides mesh refinement when the changes of value between each interval exceed the control value set. After examining the change of interval and angle values between any two adjacent grids, a new grid is added by halving marked intervals if needed. A typical grid size ranges from 0.01 cm to 1 cm through the whole domain. Thus there are more grid points for regions of large slopes or high curvatures, for temperature and species in their spatial profiles.

2.3. Chemical reaction mechanism

The chemical reaction mechanism used in this work is based on GRI-Mech 1.2[24]. GRI-Mech is a detailed chemical reaction mechanism for methane chemistry (excluding nitrogen chemistry). It includes elementary chemical reactions with corresponding rate constant expressions, which have been

mostly studied in the laboratory. GRI-Mech contains thermodynamics data including the molar heat capacity, entropy and standard enthalpy of formation values for the species. GRI-Mech 1.2 has 177 elementary reaction steps with 32 species.

Chemiluminescence intensity of the electronically excited CH species, CH*, is added to GRI-Mech. For the experiments, CH* is imaged at 431.2nm with a visible camera[25].

CH* can be produced:

$C_2H + O_2 \rightarrow CH^* + CO_2$ [26]

$C_2 + OH \rightarrow CH^* + CO$ [27]

However, CH* also may disappear in the quenching steps:

$CH^* + M \rightarrow CH + M$ [28]

$CH^* + O_2 \rightarrow CH + O_2$ [25]

And by photon emission:

$CH^* \rightarrow CH + h\nu$ [29]

where h is the Plank's constant, ν the emission frequency, and M the collision partner.

When H_2/CH_4/He is simulated, helium is added to the mechanism by assuming the role of argon, but with the appropriate third body efficiency factors.

Chapter 3

Radiation Model

In order to understand the role of radiation on flame dynamics and extinction, flame structure and response without radiation, with radiation using the optically thin approximation, and with radiation using the optically thick are computationally investigated.

3.1. Raditive transfer model

In Equation (2b), the energy equation is given as:

$$\rho A\frac{\partial T}{\partial t}+\dot{m}\frac{\partial T}{\partial r}-\frac{1}{C_P}\frac{\partial}{\partial r}\left(A\lambda\frac{\partial T}{\partial r}\right)+\frac{A}{C_p}\sum_{k=1}^{K}\rho Y_k V_k Cp_k\frac{\partial T}{\partial r}+$$
$$\frac{A}{C_p}\sum_{k=1}^{K}\dot{\omega}_k h_k w_k+\frac{A}{C_P}\dot{q}_{rad}=0$$

In the equation, $\dot{q}_{rad}$ is the heat loss per unit volume. q_{rad} is the heat flux as a function of radiation intensity I ,

$$q_{rad}(r)=\int_{4\pi} I(r,\hat{s})\hat{s}d\Omega \qquad (3a)$$

where $\hat{s}$ is the unit direction vector, and Ω the solid angle.

From the equation we can see that the radiation term is dependent on the spectral location including direction and angle information. All radiative transfer modeling relates the change of radiation intensity I_ν to local

absorption k_ν , volume emission j_ν and scattering coefficient $\sigma_{s,\nu}$. The optically thickness of a layer determines the fraction of the radiation intensity passing through the layer. Radiation traversing a medium will be weakened by the interactions with other objects. The spectral extinction coefficient β_ν , consists of the absorption coefficient k_ν and the scattering coefficient $\sigma_{s,\nu}$:

$$\beta_\nu = k_\nu + \sigma_{s,\nu} \tag{3b}$$

In the simulation, we assume the medium only absorbs and emits but not scatters. Thus, $\beta_\nu = k_\nu$.

3.2. Optically thin approximation

For the optically thin model, radative heat loss per unit volume is shown as[30]:

$$\dot{q}_{rad} = 4\pi \int_0^\infty \kappa_{p\eta}(T)(I_{\eta b}(T) - I_{\eta b}(T_\infty))d_\eta \tag{3c}$$

Where κ_η is spectral absorption coefficient, and $I_{\eta b}$ the spectral black body radiation intensity. The gray gas property model with total Planck mean absorption coefficient, α_p is applied. The Equation (3c) is simplified to:

$$\dot{q}_{rad} = 4\alpha_p \sigma(T^4 - T_\infty^4) \tag{3d}$$

where σ is the Stefan–Boltzmann constant. In the optically thin approximation, heat loss due to radiation is regarded to be emitted from CH_4, CO, CO_2, and H_2O only.

3.3. Optically thick approximation

In the optically thin region, the source term is the spontaneous emission of the medium, which results in straight line propagation of photons. In the optically thick region, the source term is the space-time gradient of the Plank function. In this work, radiative transfer including both absorption and emission are numerically calculated by using the statistical narrow-band (SNB) model with inverse line strength distribution.[31]

In the SNB model, the gas transmissivity, τ_ν , over a path *L*, is given as:

$$\tau_\nu = \exp\left[-\frac{\pi B}{2}\left(\sqrt{1+\frac{4SL}{\pi B}}-1\right)\right], \tag{3e}$$

where $B = 2\bar{\beta}_\nu / \pi$, $S = \bar{k}_\nu Xp$, and $\bar{\beta}_\nu = 2\pi\bar{\gamma}_\nu / \bar{\delta}_\nu$ are the SNB parameters for CO, CO_2, and H_2O. The bandwidth is 25 cm^{-1} for the temperatures and spectral ranges of 300-2900 K and 150-9300 cm^{-1}, respectively.[32]

Chapter 4

Kinetic Extinction

4.1. Results

One of the issues in this work is to study the flame behavior of kinetic extinctions. Since the mechanism does not involve radiative loss (as confirmed by the simulations), the flame was simulated as adiabatic. Different cases are examined to find the kinetic extinction limits as shown in Table 4.1:

Table 4.1: Test matrix for studying kinetic extinction limit.

Case Number	Fuel mole fraction (%)			Oxidizer mole fraction (%)		Volumetric Flow rate (cc/s)
	H_2	CH_4	N_2	O_2	N_2	
1a	25	20	55	10	90	1.5->0.5 after 5 sec
1b	25	20	55	10	90	1.5->0.6 after 5 sec
1c	25	20	55	11	89	1.5->0.5 after 5 sec
1d	25	20	55	10	90	1.5->0.5 after 10 sec
1e	25	20	55	9.9	90.1	1.5->0.5 after 10 sec

There are 5 cases in the table, and all of them have the same fuel mixture, which is 25%H_2-20%CH_4-55%N_2. Different ambient oxidizer mole fractions and flow rate conditions are investigated. Case 1a is the kinetic extinction case for 10%O_2/90%N_2 ambient environment. The burning lasts 5 seconds after ignition at 1.5 cc/s volume flow rate, which is then suddenly reduced to 0.5 cc/s. Peak flame temperature right before extinction is 1216K. In the simulation, burner size is set to be 0 cm so that no heat is lost to the "burner". Thus, the flame standoff distance is exactly the flame radius. Right before extinction, flame radius as predicted by instantaneous location of peak temperature (max T) is 0.556 cm, and flame radius as predicted by instantaneous location of peak photon emission from the CH* species (max CH*) is 0.534cm.

The reason for keeping the flame burning at 1.5 cc/s for 5 seconds is that by doing so, the flame spreads closer to steady state before transition of flow rate to seek the kinetic extinction condition. After a quasi-steady-state flame is established, kinetic extinction can be obtained by reducing the volumetric flow rate. If a constant volumetric flow rate of 0.5 cc/s is set at the beginning, the condition may already be below the kinetic extinction threshold, so no flame may be established.

For Case 1b, the same fuel mixture and ambient oxidizer mole fraction as for case 1a are investigated. Instead, the volumetric flow rate is reduced to 0.6 cc/s after 5 seconds of burning, with an initial 1.5 cc/s volumetric flow

rate. This allows us to examine the role of the established flame structure prior to flow rate reduction with respect to kinetic extinction. For Case 1c, the same fuel mixture and mass flow rates are used as case 1a, except the oxidizer mole fraction is set to 1% more percentage point of oxygen than for case 1a. Both cases 1b and 1c are designed to better determine quantitatively the kinetic extinction condition.

Figure 4.1 shows flame temperature versus time plots for case 1a, 1b, and 1c. After the volumetric flow rate is reduced at 5 seconds, case 1a displays a sudden temperature drop at approximately 17s, which is considered as flame extinction. In cases 1b and 1c, both flames experience sustained burning after 5 seconds. For case 1b, the flame is sustained because the volumetric flow rate is higher than for case 1a after 5 seconds, thus the *Da* number did not reach to the low limit to extinguish the flame. The peak flame temperature is 1266K at 30 seconds as the flame approaches steady state. The flame front radius is 0.611cm (max T) and 0.592cm (max CH*) at 30 seconds.

For case 1c, the flame is sustained because on the oxidizer side, the oxygen mole fraction is higher, resulting in a flame temperature that is about 100K higher than for case 1a prior to extinguishment, as seen in Figure 4.1.Peak flame temperature is 1341K at 30 seconds. Flame radius is 0.463cm (max T) and 0.450cm (max CH*) at 30 seconds.

Figure 4.2 shows the flame structure (temperature and species profiles) of 3 cases at the time case 1a is extinguishing (around 17s). Flame radii of the three cases are very close. However, flame temperatures are found to be different, being sufficiently lower for case 1a than for the other two cases. In addition, flame structure of case 1a is narrower than for the other two cases. These factors contribute to the flame extinction of case 1a.

Figure 4.3 shows flame temperature versus time for cases 1a, 1d, and 1e, as given in the Table 4.1. For both cases 1d and 1e, initial burning at 1.5 cc/s volumetric flow rate lasts 10 seconds before the step down in flow rate. Case 1d and case 1a have the same fuel mixture, oxidizer mole fraction, and volumetric flow rates, other than the initial flow rate duration. For case 1d, the flame is sustained at 1.5 cc/s for longer duration, allowing flame temperature to become higher, flame size to get larger, and flame front position to get closer to steady state before the flow rate reduction at 10 s (instead of 5 s for case 1a). The flame temperature is 1231K at 30 seconds. The flame radius is 0.548cm (max T) and 0.528cm (max CH*) at 30 seconds. Thus, the flame structure prior to mass flow rate reduction greatly impacts whether the quasi-steady kinetic extinction is realized. As can be seen, the extinction for case 1a is transient extinction due to a “weak” (or non-quasi-steady) starting condition prior to mass flow reduction, rather than quasi-steady kinetic extinction.

For case 1e, apart from changing the duration of the starting flow rate from 5 seconds to 10 seconds at 1.5 cc/s volumetric flow rate, the oxygen mole fraction is also decreased by 0.1% percentage points. As seen in Figure 4.3, the flame temperature for case 1e is just a bit higher than that for case 1a and a bit lower than that for case 1d, prior to inward flame front movement corresponding to mass flow rate reduction. As mentioned before, lower concentration of oxygen in the oxidant results in lower characteristic flame temperature. After the flame shrinks for case 1e, the flame temperature drops more than for case 1a, leading to extinguishment even faster than for case 1a. Flame extinction is obtained at around 16 seconds. The flame temperature is 1223K, and the flame radius is 0.574cm (max T) and 0.552cm (max CH*), right before flame extinction.

4.2. Discussion and Conclusions

There are some conclusions that can be drawn from the cases examined in Table 4.1. We chose the 4.5-second moment when the flame is sustained by1.5 cc/s volumetric flow rate and close to steady state to study flame dynamics and behaviors under different conditions.

Table 4.2: Adiabatic flame temperature and flame radius comparison of different conditions with 25%H_2-20%CH_4-55%N_2 fuel mixture at 4.5 second.

Case Number	T_{ad} (K)	$R_{max\ T}$ (cm)	$R_{max\ CH^*}$ (cm)
1a, 1b, 1d	1305	1.16	1.14
1c	1385	1.10	1.08
1e	1303	1.16	1.14

Since cases 1a, 1b, and 1d have the same starting flow rate and oxidizer mole fraction, we list these 3 cases together. For case 1c, there is less oxidizer dilution than for Cases 1a, 1b, and 1d. We can clearly see that less oxygen concentration in the oxidant results in lower adiabatic flame temperature and bigger flame size. We can verify this through the comparison of cases 1a and 1e. Since oxygen mole fraction for case 1e is only 0.1% percentage points less than that for case1a, difference between flames sizes of the two cases is small. We can explain the difference based on adiabatic flame temperature. More oxygen in the ambient means more heat release, raising the flame temperature in the flame sheet. Thus, the adiabatic flame temperature is higher with more oxygen mole fraction in the oxidant. On the other hand, since the stoichiometric ratio equals 1 at the diffusion flame sheet, less oxygen in the ambient air makes flame size bigger (more area at the flame front) in order to seek more oxygen to react with fuel.

There is no heat loss for the adiabatic flame, thus the adiabatic flame temperature and flame radius are close to the adiabatic steady-state value as

time passes. In addition, we also obtained that without radiative loss, the flame radius (max T) is larger than the flame radius (max CH*) for the cases.

One thing that needs to be mentioned is that kinetic extinctions can be obtained at oxygen mole fractions larger than 10%, for more diluted fuel mixtures. However, for real cases where the actual burner size is 0.375 cm in radius, the corresponding flame radii at extinction would be greatly affected by the presence of the burner. Thus, flame radii at extinction which are about double the size of the burners to be utilized are desired. As a result, only ambient oxygen mole fractions ~10% or less produce the desired flame sizes, for the fuel mixture examined.

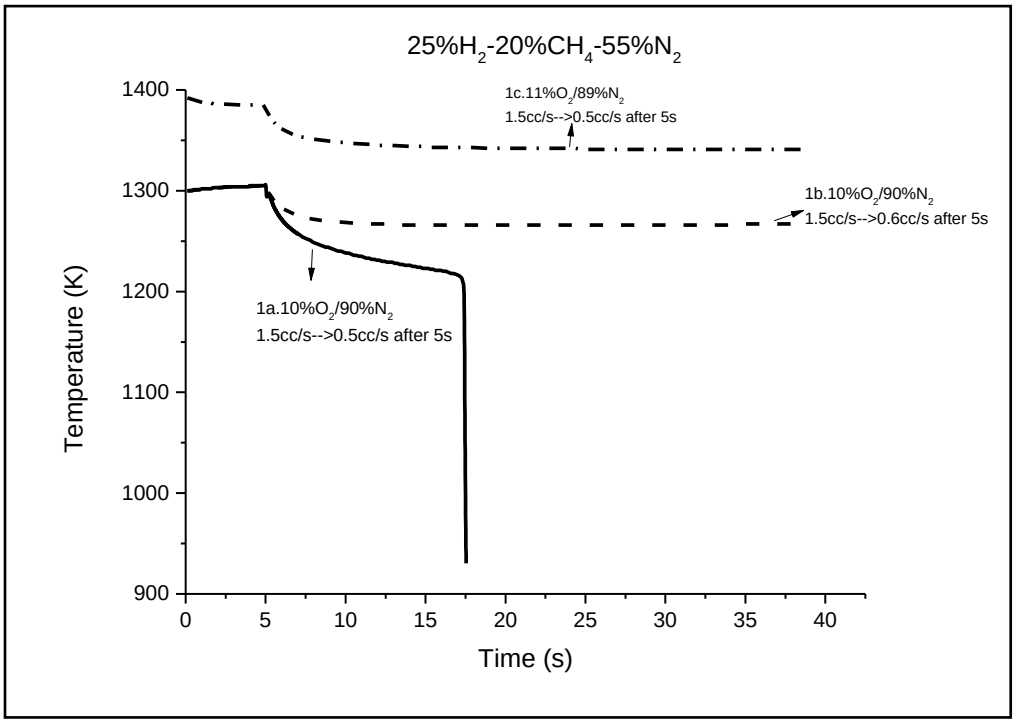

Figure 4.1: Flame temperature versus time of kinetic extinction limit case and its comparison cases part1.

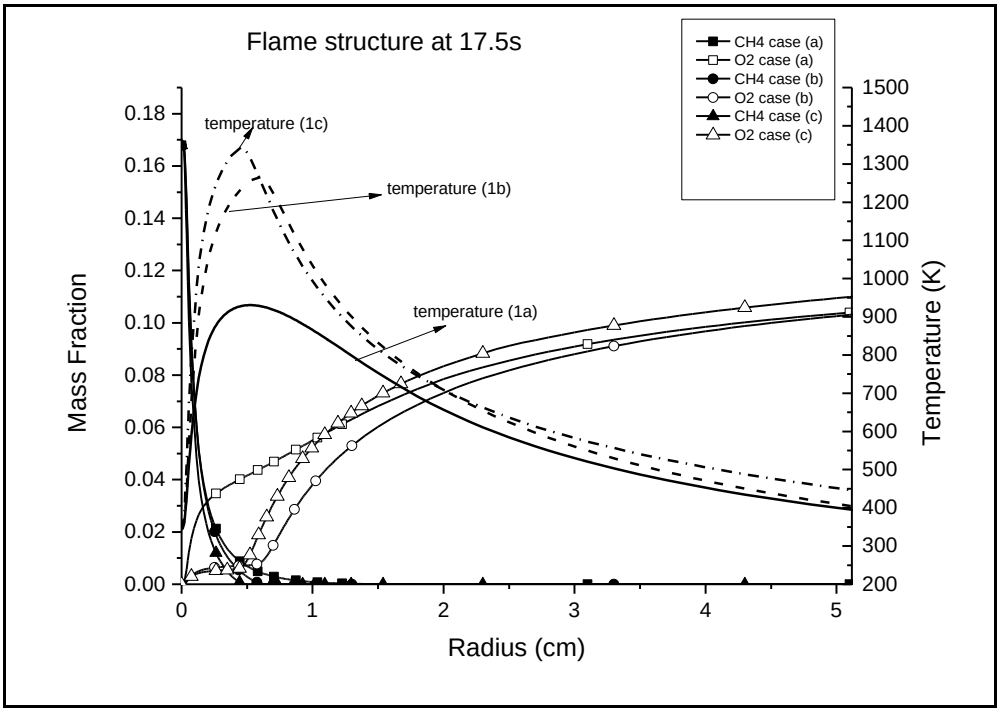

Figure4.2: Flame structure of kinetic extinction limit case and its comparison cases part 1.

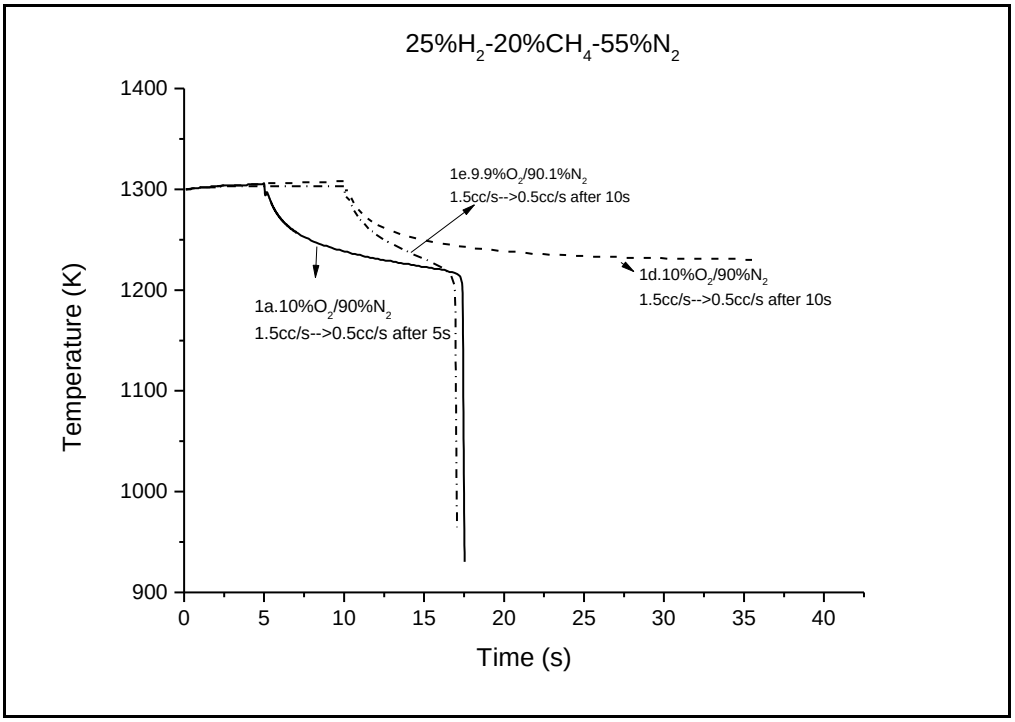

Figure4.3: Flame temperature versus time of kinetic extinction limit case and its comparison cases part 2.

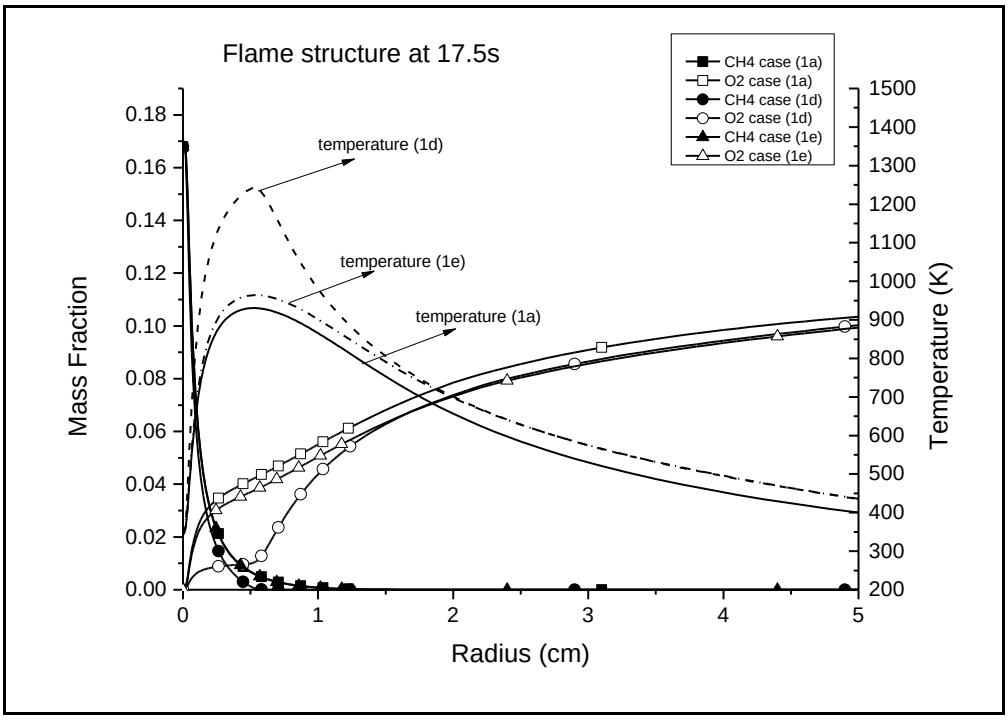

Figure4.4: Flame structure of kinetic extinction limit case and its comparison cases part 2.

Chapter 5

Radiative Extinction

Another issue in this work is to study flame behavior at raditive extinction. Both optically thick and optically thin approximations are applied to simulate the flame behavior. Optically thick approximations result in flame dynamics that are closer to actual experimental data than those for optically thin approximations.[1]

5.1. Results of radiative extinctions with optically thick approximations

Table 5.1: Test matrix of radiative extinctions using optically thick approximations with $H_2/CH_4/N_2$ fuel mixtures.

Case Number	Fuel mole fraction (%)			Oxidizer mole fraction (%)		Volumetric Flow rate (cc/s)
	H_2	CH_4	N_2	O_2	N_2	
2a	25	20	55	21	79	5
2b	20	25	55	21	79	5
2c	30	15	55	21	79	5
2d	0	45	55	21	79	5

A test matrix to examine radiative extinctions with optically thick approximations, as shown in Table 5.1.

All of the cases resulted in extinction caused by reduction in total enthalpy (and flame temperature) due to radiative heat loss. Cases in Table 5.1 are all conducted in $21\%O_2/79\%N_2$ atmospheric air. Different fuel mixtures of $H_2/CH_4/N_2$ are investigated to study the different flame dynamics and behaviors.

Figure 5.1 shows flame temperature versus time at 5 cc/s volumetric flow rate for cases 2a, 2b, 2c, and 2d. For case 2a, the flame temperature right before extinction is about 1213K at 4.96 seconds. For case 2b, the flame temperature before extinction is about 1224K at 3.73 seconds. For case 2c, the flame temperature before extinction is about 1172K at 7.63 seconds. For case 2d, the flame temperature before extinction is about 1285K at 1.96 seconds. It can be seen that the flames extinguish sooner when there is higher methane mole fraction (and lower hydrogen mole fraction) in the fuel mixture (with constant nitrogen mole fraction). The time duration until radiative extinction is highly dependent on the mixture composition. More hydrogen in the fuel mixture results in less radiative heat loss, as well as lower flame temperature before extinction.

Figure 5.2 shows flame radius versus time of radiative extinctions using optically thick approximations in atmosphere air. Case 2d has the largest flame size. Radiative heat loss increases with flame size. As mentioned, case

2d extinguishes fastest among all cases. The amount of the radiation loss from the flame is proportional to the flame volume. Big flame sizes would have more heat loss due to radiation.

Table 5.2: Test matrix of radiative extinction cases with optically thick approximation with same fuel and oxidizer mole fractions.

Case Number	Fuel mole fraction (%)			Oxidizer mole fraction (%)		Volumetric Flow rate (cc/s)
	H_2	CH_4	N_2	O_2	N_2	
3a	25	20	55	21	79	5
3b	25	20	55	21	79	10
3c	25	20	55	21	79	15

Cases in Table 5.2 are tested to investigate how the volumetric flow rate impacts the flame behavior. As seen in Figure 5.3, it takes less time to reach radiative extinction for high flow rates when other conditions are same. The flame has less heat loss due to radiation at low flow rates (smaller characteristic flame sizes), thus the time duration until extinction at lower flow rates are longer than at higher flow rates. Figure 5.4 shows flame front radius versus time plot for cases in Table 5.2. As mentioned before, large flame sizes have more heat loss due to radiation, resulting in fast extinctions. By growing larger, the flames end up killing themselves.

Table 5.3: Test matrix of radiative extinction cases by comparing N_2 and He as inerts on flame behavior.

Case Number	Fuel mole fraction (%)				Oxidizer mole fraction (%)			Volume flow rate (cc/s)
	H_2	CH_4	N_2	He	O_2	N_2	He	
4a	20	25	55	0	21	79	0	5
4b	20	25	55	0	21	79	0	10
4c	20	25	0	55	21	0	79	5
4d	20	25	0	55	21	0	79	10

Table 5.3 shows the test matrix cases of using different inert gases in both fuel and oxidizer sides to compare flame behavior. The different inerts, i.e. N_2 versus He, are chosen to assess transport (e.g. diffusive properties) effects on flame response and stability. For example, He can induce the pulsating instability for Lewis number (*Le*)> 1. The fuel components and their relative compositions are the same for the two sets, with different inert species in balance; similarly, the ambient composition reflects the use of a different inert species in the fuel mixture. Since the molar heat capacity of diatomic nitrogen is higher than that of monatomic helium, the characteristic flame temperatures will be different. This, in turn, affects the Zeldovich number (*Ze*), which will be different for the two experimental sets, influencing stability and extinction.

Figure 5.5 shows the flame temperature comparisons for the tested cases. As expected, He cases have higher flame temperatures, but, unexpectedly,

extinguish faster than N_2 cases. As previously mentioned, He cases have higher flame temperature because the molar heat capacity of helium is lower than diatomic hydrogen (and nitrogen), and thus less heat is needed to increase the temperature of the mixture. Figure 5.6 shows that at the same volumetric flow rate, He and N_2 cases have almost the same flame radius before extinguishing. Since He is an inert noble gas, it is not involved in any chemical reactions like nitrogen can be. Nevertheless, assuming that the chemical production rates are both zero for nitrogen and helium, the heat release rates in cases 4a and 4c should be the same. It is not immediately clear why He cases extinguish faster than N_2 cases. Thermal-diffusive transport effects likely play a role, and more investigation is needed. When the volumetric flow rate is increased, the extinction time of He cases and N_2 cases become closer.

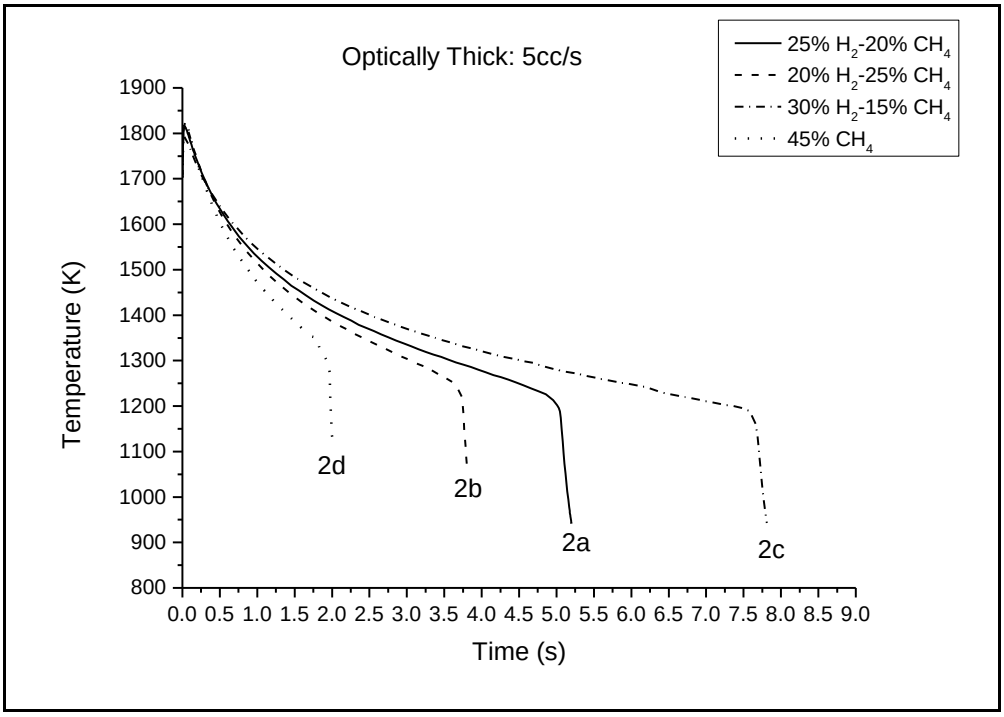

Figure 5.1: Flame temperature versus time of radiative extinctions using optically thick approximations at 5cc/s.

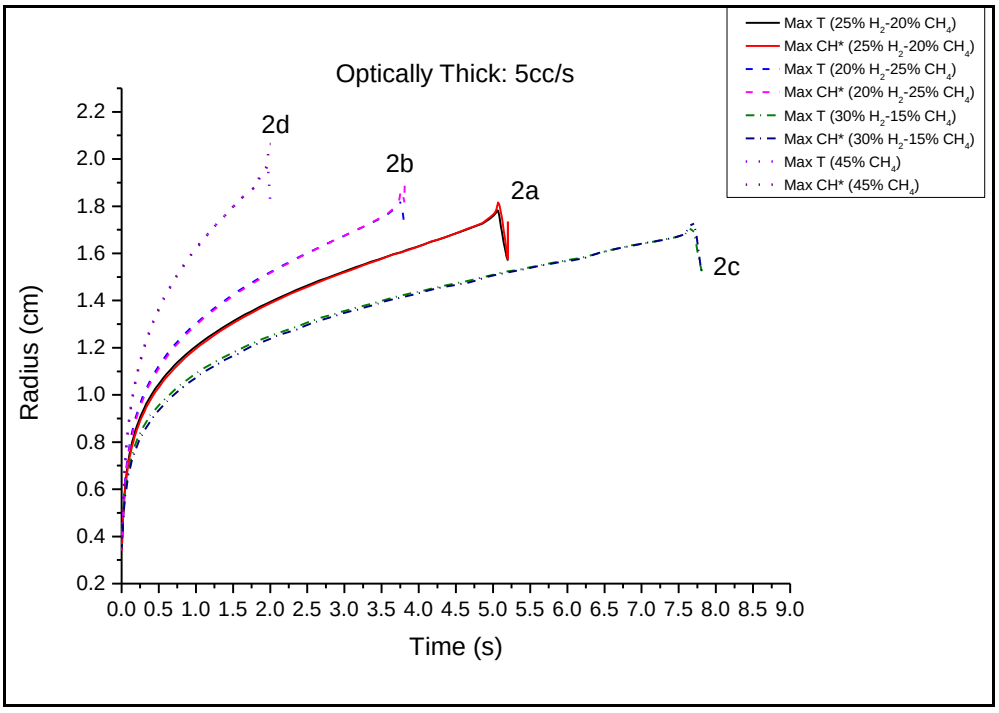

Figure 5.2: Flame radius versus time of radiative extinctions using optically thick approximations at 5cc/s.

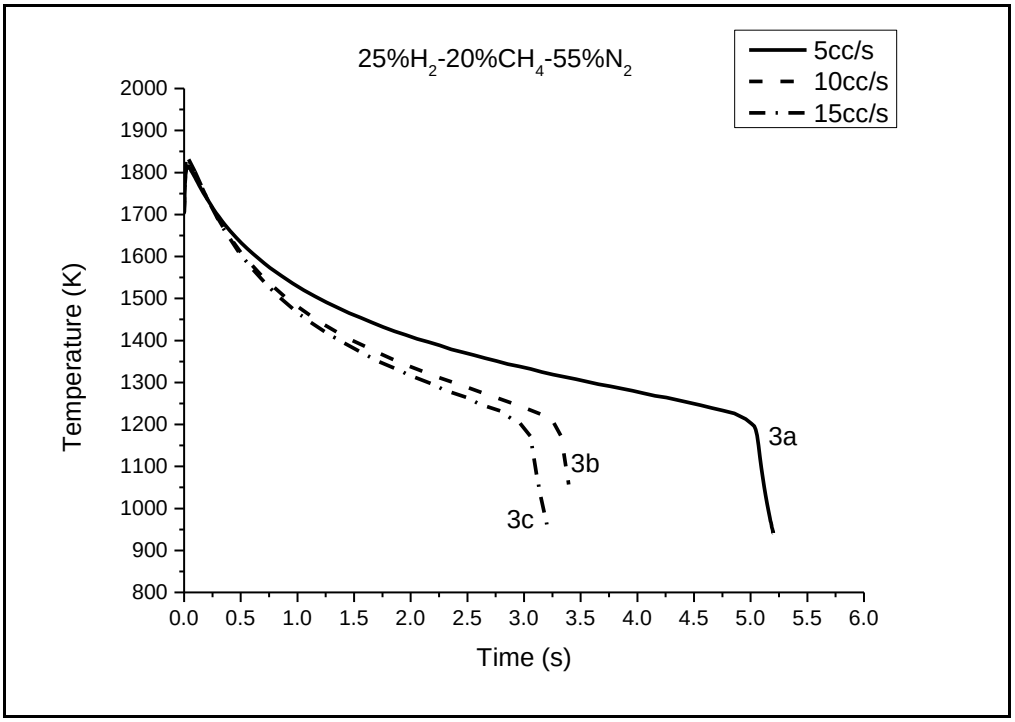

Figure 5.3: Flame temperature versus time of radiative extinctions with same fuel and oxidizer mole fractions.

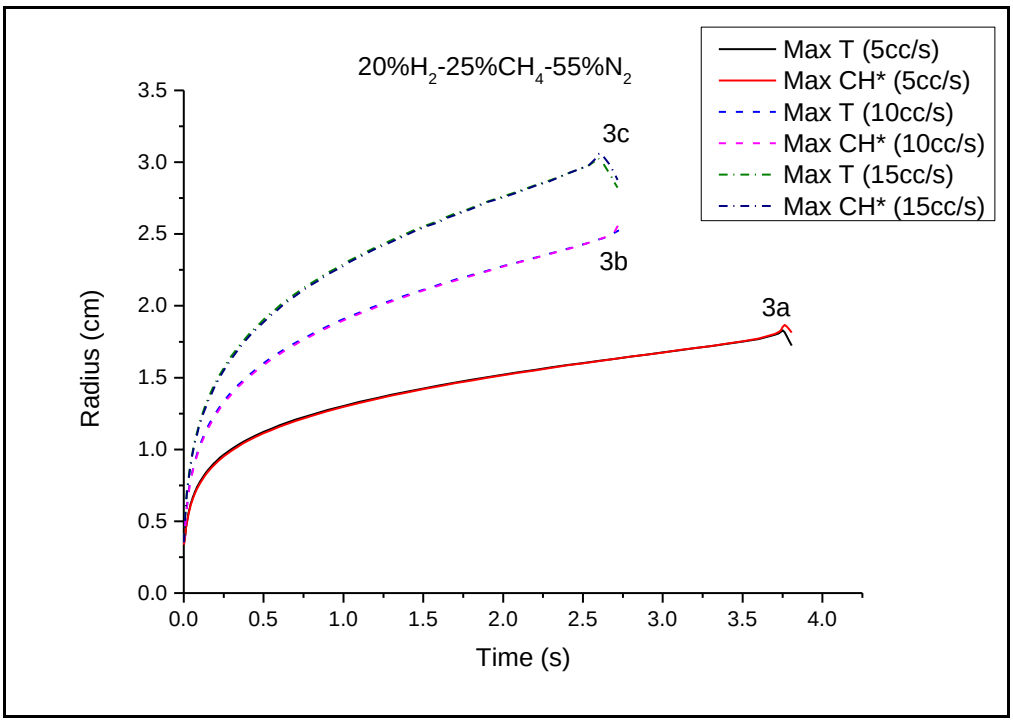

Figure 5.4: Flame radius versus time of radiative extinctions with same fuel and oxidizer mole fractions.

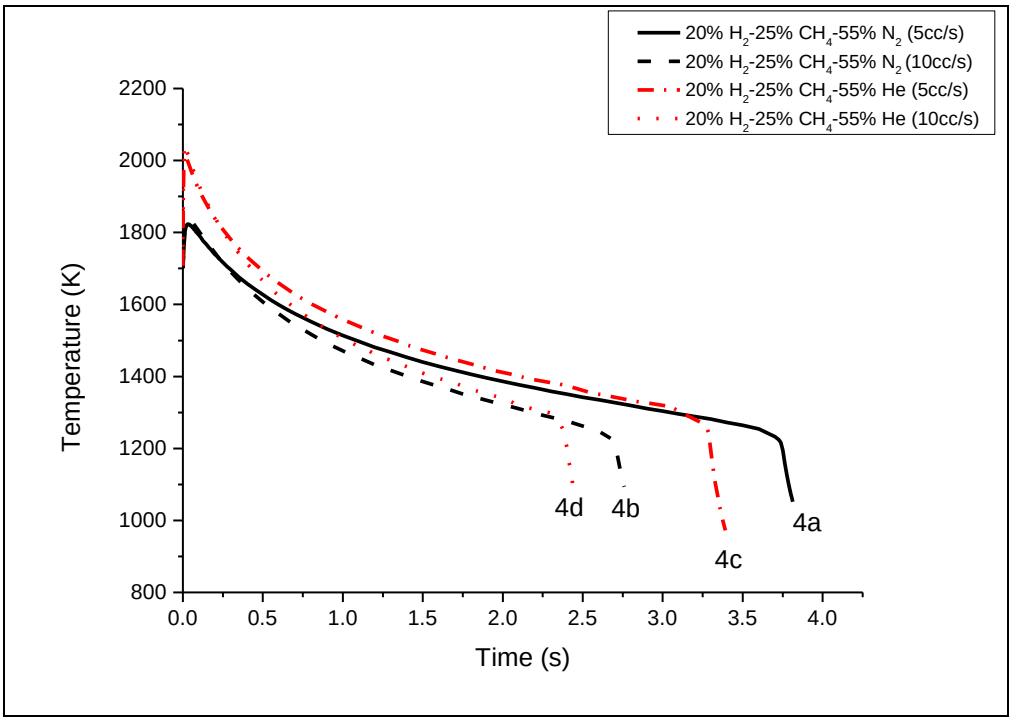

Figure 5.5: Comparison of flame temperatures using N_2 versus He as inert, employing the optically thick approximation.

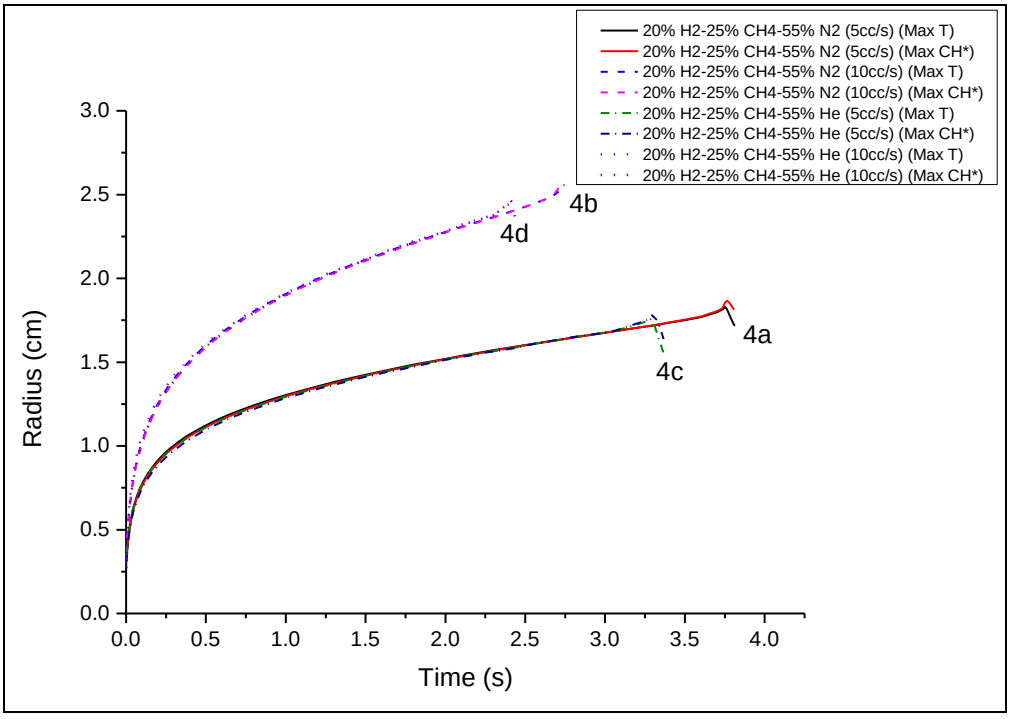

Figure 5.6: Comparison of flame radii evolution using N_2 versus He, employing the optically thick approximation.

5.2. Comparison of optically thin and optically thick approximations.

As shown in previous work with comparisons between experiments and computations, the optically thin approximation may not be accurate in assessing radiation effects, especially with respect to flame extinction. In this work, we examine the optically thin approximation to compare flame behaviors obtained using the optically thick approximation.

Figure 5.7 compares optically thick and optically thin approximations introducing 30%H_2-15%CH_4-55%N_2 fuel mixture into atmospheric air. Both approximations manifest radiative extinctions at the same volumetric flow rates. Flame temperatures before extinction in optically thick cases are close to those in optically thin cases. It takes longer to reach extinction for optically thick cases than it does for optically thin cases. One reason is that in the optically thick approximation, heat reabsorption is taken into account, making the flame more "adiabatic," while in the optically thin cases, radiative heat loss is overestimated. This can be seen in Figure 5.8, where the flame radii in optically thin cases are bigger than those in optically thick cases, due to the density difference.

Figure 5.9 compares the flame structures (temperature and key species profiles) at the moment just before extinction of optically thick and optically thin cases. The peak temperatures of both cases are very close. Nevertheless,

due to heat reabsorption, the temperature distribution along the flame radius of the optically thick case is wider than that of the optically thin case.

5.3. Discussion and conclusions

For radiative cases, at the same fuel mixture and volumetric flow rate issuing into atmospheric air, higher hydrogen mole fraction in the $H_2/CH_4/N_2$ fuel mixture is characterized by longer extinction times. Flame temperatures just before radiative extinction are found to be lower in the cases having longer extinction times. Flame radii just before radiative extinction are small in the cases characterized by long extinction times. Less heat loss from radiation makes the extinction time longer. Flame temperature goes up for a very short period of time before heat losses become large enough to decrease the flame temperature. After the rise, the flame temperature continues decreasing until extinction in the radiative case. Less heat loss, i.e. radiative reabsorption, makes this process last longer, and thus the flame front spreads more slowly.

At low flow rate, extinction time decreases as flow rate increases. When the flow rate keep increasing, the differences between extinction times become less apparent, thus the differences of flame temperatures and sizes before extinction are small as well.

When employing He as inert in both fuel and oxidizer mixtures, the flame temperatures increase due to the lower molar heat capacity of helium.

In addition, the diffusion coefficients of helium and nitrogen are very different. Interestingly, the flame radii are close for the two cases.

For both optically thin and optically thick cases, flame radii predicted by peak temperature and by peak photon emission from CH* species are very close to each other. Optically thick cases display longer extinction times and smaller flame sizes compared with optically thin cases. The optically thick cases, with radiative reabsorption, should be more accurate and closer to the experimental results.

When taking radiation into account, flame extinction is mainly due to lower enthalpy ultimately resulting in reactant leakage. Radiative heat loss lowers the flame temperature, resulting in higher density for more fuel accumulation. However, as the flame continues to expand and decrease in temperature, the effect of enhanced mass storage ability cannot counteract for that of decreasing reaction rates, pushing the flame to spread outwardly faster (than the adiabatic case) in order to reduce the fuel mass flux into its consumption zone (as seen from the Lagrangian reference frame of the flame front). Eventually, heat loss due to radiation lowers the heat release rate until the flame temperature is so low that there is reactant leakage, and the flame extinguishes. A high flow rate can result in a maximum extinction system *Da* number beyond which burning is not possible, caused by the significant reduction of temperature.

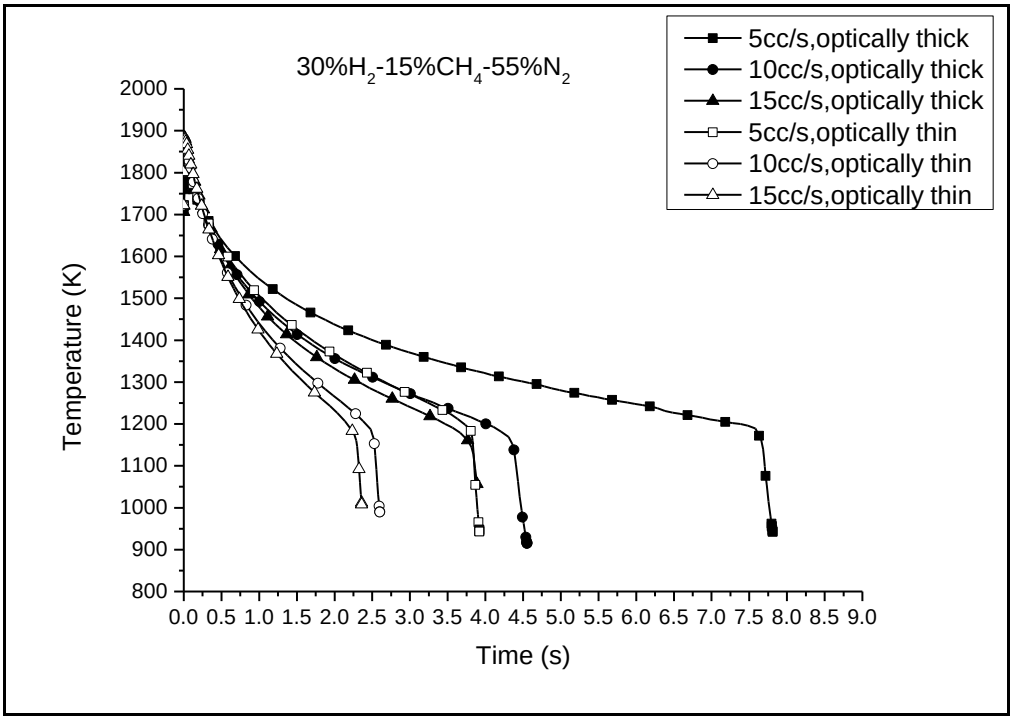

Figure 5.7: Flame temperature versus time for 30%H_2-15%CH_4-55%N_2 mixture, employing optically thick and optically thin approximations.

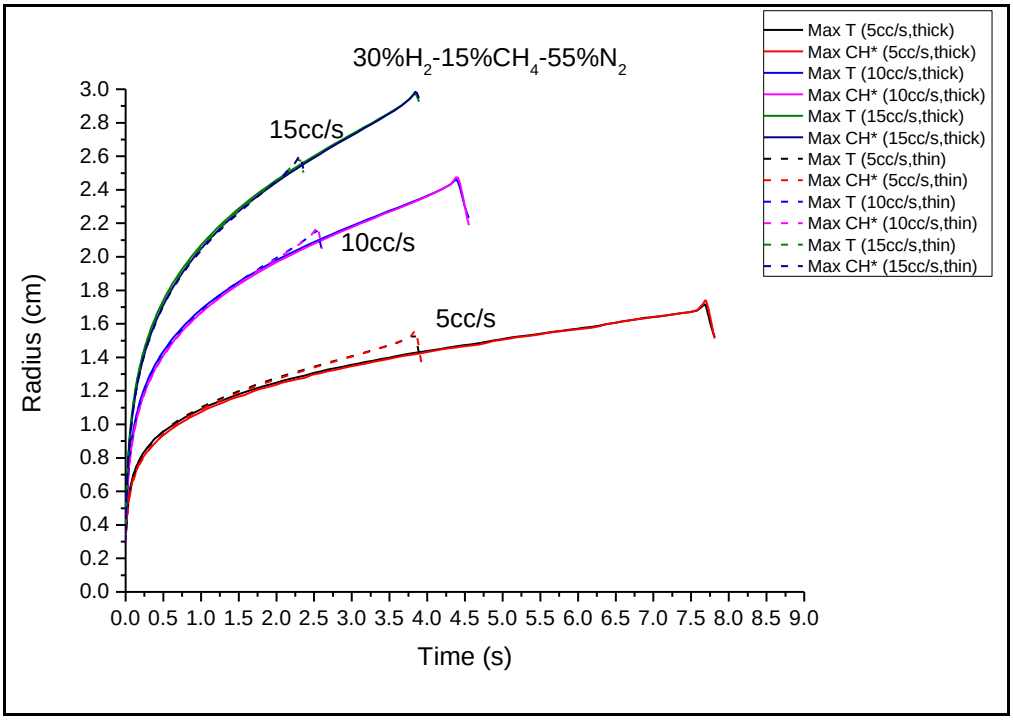

Figure 5.8: Flame radius versus time for 30%H_2-15%CH_4-55%N_2 mixture, employing optically thick and optically thin approximations.

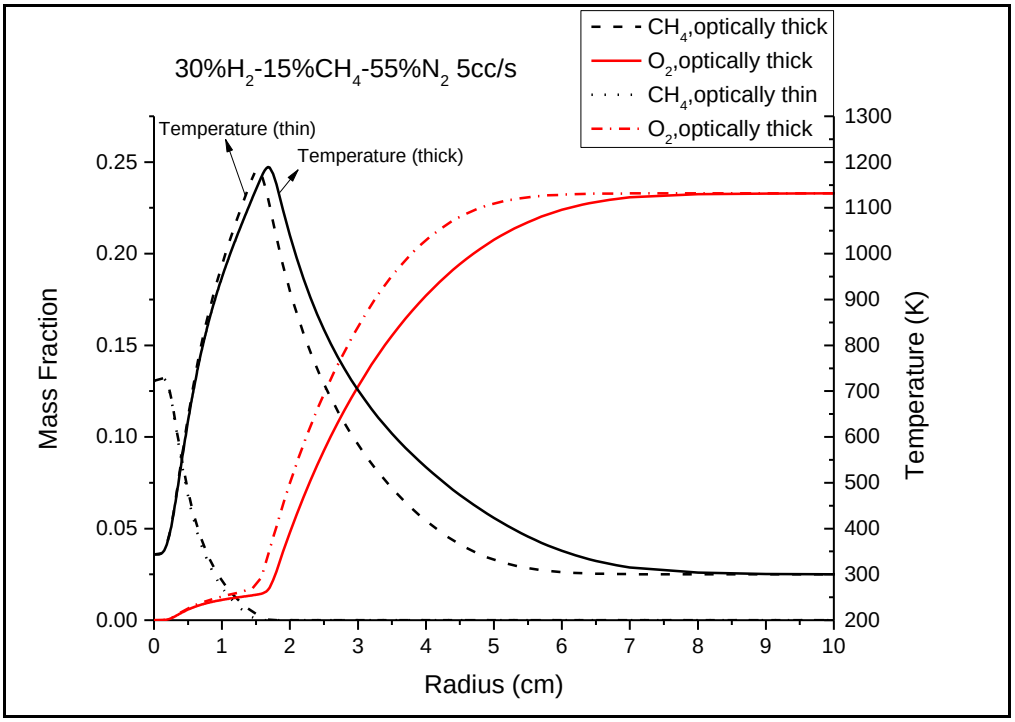

Figure 5.9: Comparison of flame structures just before extinction with optically thin and optically thick approximations.

Chapter 6

Concluding Remarks

This thesis presents computational simulations of one-dimensional spherical diffusion flame responses and structures under microgravity conditions. The basic flame configuration adopted for the investigations is the spherically-symmetric diffusion flame generated by issuing a fuel mixture into a quiescent oxidizing environment. Appropriate modifications have been made to the mass, energy, and species governing equations, along with initial conditions, in the previous code. Burner size is set to zero to eliminate heat loss effects to the burner, better isolating kinetic extinction limits. Optically thin and optically thick approximations are compared in solving the radiative transfer equations to assess radiative extinction. Different fuel mixtures are tested to study the different flame behaviors for kinetic and radiative extinctions.

6.1. Review of results and conclusions

Many factors such as fuel mixture, oxidizer mixture, and mass flow rate influence the dynamics and extinction processes of spherical diffusion flames. While chemical kinetics does not need to be considered in the limit of flame-sheet burning for a diffusion flame, it is of critical importance in

extinction processes. Thus the investigation of extinction processes affords an additional means to examine flame chemistry, as well as transport models. From practical considerations, extinction is a key phenomenon in combustion processes that needs to be understood and controlled. A summary of the results and conclusions from this work are given below.

For kinetic extinctions, a certain flow rate is applied to ignite and establish a quasi-steady flame, and then the flow rate is abruptly lowered (below the steady-state extinction limit) to seek the purely kinetic extinction limit, as the flame responds quasi-steadily. Dilution on oxidizer side is employed to ensure that the flame size just before extinction is about double the radius of the burner to be utilized. Effect of starting flow rate duration time to establish a quasi-steady flame is evaluated with respect to how the flame responds to flow rate reduction and subsequent extinction.

For radiative extinctions, $H_2/CH_4/N_2$ and H_2/CH_4/He fuel mixtures are examined for different mole fractions compositions and issuing flow rates. Heat loss due to radiation is the dominant factor causing extinction as the flame spreads outwardly, when there is no steady solution for the given fuel and ambient mixtures. Extinction time varies less at high flow rates compared to low flow rates, for a given fuel mixture. High hydrogen concentration in the fuel mixture extends the extinction time, due to the high reactivity and diffusivity of hydrogen. For the same mole fraction of dilution in the fuel mixture and oxidizer mixture ambient, the one that is diluted by helium

extinguishes sooner than the one contains nitrogen. Optically thin models are shown to have shorter extinction times and bigger flame sizes than optically thick models due to more heat loss.

6.2. Suggestions for future work

Constant volume conditions (e.g. using a chamber) can be examined and compared with constant pressure cases for both kinetic and radiative extinction studies. Maximum extinction system *Da* number in radiative cases can be found at high flow rates beyond which burning is not possible. Different fuel mixtures can be tested in different fuel molar fractions such as C_2H_4/N_2, C_2H_4/He etc. CO_2dilution cases can be compared with N_2 and He, to assess radiative reabsorption. Different chemical kinetic mechanisms can be applied to assess key reaction routes.

References

[1] S. D. Tse, D. Zhu, C. J. Sung, Y. Ju, and C. K. Law, Microgravity burner-generated spherical diffusion flames: experiment and computation, *Combustion and Flame*, 125: 1265-1278, 2001

[2] C. K. Law, S. D. Tse, K. R. Sacksteder, Structure and response of spherical and diffusion flames (s-Flame), *Science Requirements Documents for a Space Flight Experiment*, 2010

[3] A. Atreya and S. Agrawal, Effect of radiative heat loss on diffusion flames in quiescent microgravity atmosphere, *Combustoin and Flame*, 115: 372-382, 1998

[4] T. H. Cochran, Combustion Experiments in a Zero-Gravity Laboratory, *AIAA progress in Astronautics and Aeronautics*, 73, 1981.

[5] P. D. Ronney, Effect of Gravity on Laminar Premixed Gas Combustion I: Flammability Limits and Burning Velocities, *Combustion and Flame*, 62: 107-119, 1985

[6] C. K. Law and G.M. Faeth, Opportunities and challenges of combustion in Microgravity, *Prog. Energy Combust. Sci*., 20: 65-113, 1994

[7] A. Atreya, S. Agrawal, T. Shamim, K. Pickett, K. R. Sacksteder and H. R. Baum, Radiant extinction of gaseous diffusion flames, *Third International Microgravity Combustion Workshop*, Cleveland, 319-325, 1994

[8] A. Atreya, S. Berhan, M. Chernovsky, and K. R. Sacksteder, Unsteady spherical diffusion flames in microgravity, *Sixth International Microgravity Combustion Workshop*, Cleveland, 113-116, 2001

[9] P. B. Sunderland, R.L. Axelbaum, D.L. Urban, B.H. Chao and S. Liu, Effects of structure and hydrodynamics on the sooting behavior of spherical microgravity diffusion flames, *Combustion and Flame*, 132: 25-33, 2003

[10] K. Mills and M. Matalon, Extinction of spherical diffusion flames in the presence of radiant loss, *Symposium (International) on Combustion*, 27: 2535-2541, 1998

[11] E. W. Christiansen, S. D. Tse, C. K. Law, A computational study of oscillatory extinction of spherical diffusion flames, *Combustion and Flame*, 134: 327-337, 2003.

[12] C. K. Law, Combustion Physics, Cambridge University Press, New York, NY, 2005

[13] J. S. Tien, Diffusion flame extinction at small stretch rates: The mechanism of radiative loss, *Combustion and Flame*, 65: 31-34, 1985

[14] B. H. Chao, C. K. Law, J. S. Tien, Structure and extinction of diffusion flames with flame radiation, *Symposium (International) on Combustion*, 23: 523-531, 1991

[15] Liñán, A., The asymptotic structure of counterflow diffusion flames for large activation energies, *Acta Astronautica* 1:1007-1039, 1974.

[16] R. J. Kee, J. F. Grcar, M. D. Smooke, J. A. Miller, Sandia Report SAND 85-8240, *Sandia National Laboratories*, 1984

[17] C. F. Curtiss and J. O. Hirschfelder, *Journal of Chemical Physics*, 17: 550,

1949
[18] S. Chapman and T. G. Cowling, The Mathematical Theory of Non-Uniform Gases, 3rd ed., Cambridge University Press, Cambridge, 1970
[19] T. P. Coffee and J. M. Heimerl, Transport algorithms for premixed, laminar steady-state flames, *Combustion and Flame*, 43: 273-289, 1981
[20] R. J. Kee, J. F. Grcar, M. D. Smooke, J. A. Miller, and E. Meeks, Premix: A fortran program for modeling steady laminar one-dimensional premixed flames, *Sandia National Laboratories*, 1998
[21] R. J. Kee, F. M. Rupley, E. Meeks, and J. A. Miller, Chemkin-III: A fortran chemical kinetics package for the analysis of gas-phase chemical and plasma kinetics, *Sandia National Laboratories*, 1995
[22] R. J. Kee, J. Warnatz, and J. A. Miller, A Fortran computer code package for the evaluation of gas-phase viscosities, conductivities, and diffusion coefficients, *Sandia National Laboratories*, 1983
[23] J. F. Grcar, The Twopnt program for boundary value problems version 3.10, *Sandia National Laboratories*, 1992
[24] M. Frenklach, H. Wang, C. L. Yu, M. Goldenberg, C. T. Bowman, R. K. Hanson, D. F. Davidson, E. J. Chang, G. P. Smith, D. M. Golden, W. C. Gardiner, and V. Lissiansk, http://www.me.berkeley.edu/gri_mech/
[25] K. T. Walsh, M. B. Long, M. A. Tanoff, and M. D. Smooke, Experimental and computational study of CH, CH*, and OH* in an axisymmetric laminar diffusion flame, *Symposium (International) on Combustion,* 27:615-623, 1998
[26] H. Wang, S. M. Gardiner, W. C. Jr., M. Frenklach, and Y. Hidaka, *Combust. Flame* 67:65–75, 1987
[27] R. P. Porter, A. H. Clark, W. E. Kaskan, and W. E. Browne, *Proc. Combust. Inst*. 11:907–917, 1967
[28] H. Wang, S. M. Gardiner, W. C. Jr., and J. Warnatz, *Prog. Aeronaut. Astronaut*. 95:198, 1984
[29] K. H. Becker, H. H. Brenig, and T. Tataczyk, *Chem. Phys. Lett.*, 71:242, 1980
[30] S. Tang, M. K. Chernovsky, H. G. Im, and A. Atreya, A computational study of spherical diffusion flames in microgravity with gas radiation Part I: Model development and validation, *Combustion and Flame*, 157: 118-126, 2008
[31] W. Malkmus, Random Lorentz Band Model with Exponential-Tailed S-1 Line-Intensity Distribution Function, *J. Opt. Soc. Am.*, 57:323–329, 1967
[32] A. Soufiani and J. Taine, High temperature gas radiative property parameters of statistical narrow-band model for H_2O, CO_2 and CO, and correlated-K model for H_2O and CO_2, *Int. J. Heat Mass Transfer*, 40: 987-991, 1997